Physiologically Relevant Oxidative Degradation of Oligo(proline) Cross-Linked Polymeric Scaffolds

ARTICLE *in* BIOMACROMOLECULES · DECEMBER 2011

Impact Factor: 5.75 · DOI: 10.1021/bm201328k · Source: PubMed

7 AUTHORS, INCLUDING:

Shann S Yu
École Polytechnique Fédérale de Lausanne
22 PUBLICATIONS **288** CITATIONS
SEE PROFILE

Daniel S Perrien
Vanderbilt University
47 PUBLICATIONS **1,015** CITATIONS
SEE PROFILE

Todd D Giorgio
Vanderbilt University
88 PUBLICATIONS **1,932** CITATIONS
SEE PROFILE

Hak-Joon Sung
Vanderbilt University
68 PUBLICATIONS **1,145** CITATIONS
SEE PROFILE

Article

pubs.acs.org/Biomac

Physiologically Relevant Oxidative Degradation of Oligo(proline) Cross-Linked Polymeric Scaffolds

Shann S. Yu,[†,‡] Rachel L. Koblin,[†] Angela L. Zachman,[†,‡] Daniel S. Perrien,[§,∥,⊥] Lucas H. Hofmeister,[†,‡] Todd D. Giorgio,[†,‡,#] and Hak-Joon Sung*[,†,‡]

[†]Department of Biomedical Engineering, [‡]Vanderbilt Institute of Nanoscale Science and Engineering, [∥]Vanderbilt University Institute of Imaging Science, [#]Department of Chemical and Biomolecular Engineering, Vanderbilt University, Nashville, Tennessee, United States

[§]Department of Orthopaedics and Rehabilitation, [⊥]Vanderbilt Center for Bone Biology, Vanderbilt University Medical Center, Nashville, Tennessee, United States

ABSTRACT: Chronic inflammation-mediated oxidative stress is a common mechanism of implant rejection and failure. Therefore, polymer scaffolds that can degrade slowly in response to this environment may provide a viable platform for implant site-specific, sustained release of immunomodulatory agents over a long time period. In this work, proline oligomers of varying lengths (P_n) were synthesized and exposed to oxidative environments, and their accelerated degradation under oxidative conditions was verified via high performance liquid chromatography and gel permeation chromatography. Next, diblock copolymers of poly(ethylene glycol) (PEG) and poly(*ε*-caprolactone) (PCL) were carboxylated to form 100 kDa terpolymers of 4%PEG-86%PCL-10%cPCL (cPCL = poly(carboxyl-*ε*-caprolactone); *i*% indicates molar ratio). The polymers were then cross-linked with biaminated PEG-P_n-PEG chains, where P_n indicates the length of the proline oligomer flanked by PEG chains. Salt-leaching of the polymeric matrices created scaffolds of macroporous and microporous architecture, as observed by scanning electron microscopy. The degradation of scaffolds was accelerated under oxidative conditions, as evidenced by mass loss and differential scanning calorimetry measurements. Immortalized murine bone-marrow-derived macrophages were then seeded on the scaffolds and activated through the addition of *γ*-interferon and lipopolysaccharide throughout the 9-day study period. This treatment promoted the release of H_2O_2 by the macrophages and the degradation of proline-containing scaffolds compared to the control scaffolds. The accelerated degradation was evidenced by increased scaffold porosity, as visualized through scanning electron microscopy and X-ray microtomography imaging. The current study provides insight into the development of scaffolds that respond to oxidative environments through gradual degradation for the controlled release of therapeutics targeted to diseases that feature chronic inflammation and oxidative stress.

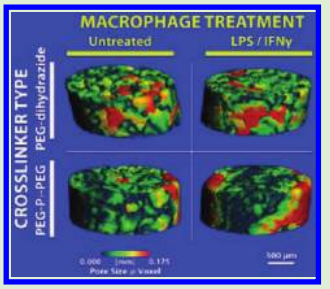

INTRODUCTION

Abnormal changes in environmental parameters, such as temperature, pH, protease activity, or redox balance, have been documented in a wide array of pathophysiological conditions.[1−5] Therefore, the development of "smart", synthetic biomaterials that are capable of responding specifically to changes in these environments holds promise in facilitating the programmed delivery of therapeutics and imaging contrast agents in a site- and timing-specific way.[6−9]

In particular, elevated levels of reactive oxygen species (ROS), such as H_2O_2 and O_2^-, are typically observed in the pro-inflammatory response to pathogens and to implanted biomaterials. In the latter case, the chronic production of ROS has been a mechanism behind implant rejection and failure, necessitating follow-up implant replacement surgeries years after the original procedure. This phenomenon has been observed for a wide array of applications, including orthopedic, vascular, and neurological implant materials.[10−12] Consequently, ROS-responsive materials would be desirable as implant coatings for such applications, to facilitate controlled local release of inflammatory modulators and suppressors without off-target side effects elsewhere in the body.

The first example of a ROS-responsive biomaterial was demonstrated by Napoli et al. using a poly(propylene sulfide) (PPS)-based system, which is initially hydrophobic but becomes oxidized into more hydrophilic sulfones by peroxides.[13] In this work, the authors self-assembled vesicles composed of PPS cores with hydrophilic poly(ethylene glycol) (PEG) coronas. Within a few hours of H_2O_2 addition, the vesicles exhibited a hydrophobic-to-hydrophilic transition, a behavior that can be leveraged for controlled release applications. These materials have now begun to see applications in immunobioengineering, leading to new vaccine nanoparticles that have been validated in vivo in mouse models.[14−16] At the same time, it may also be desirable to produce materials that respond to oxidative environments with slower changes in material properties.

The accumulation of oxidatively modified proteins has been demonstrated as a hallmark of the aging process and also in certain diseases.[17,18] Within such proteins, the amino acids

Received: September 22, 2011
Revised: October 21, 2011
Published: October 23, 2011

Scheme 1. Synthesis of Biaminated PEG-P$_n$-PEG Cross-Linkers

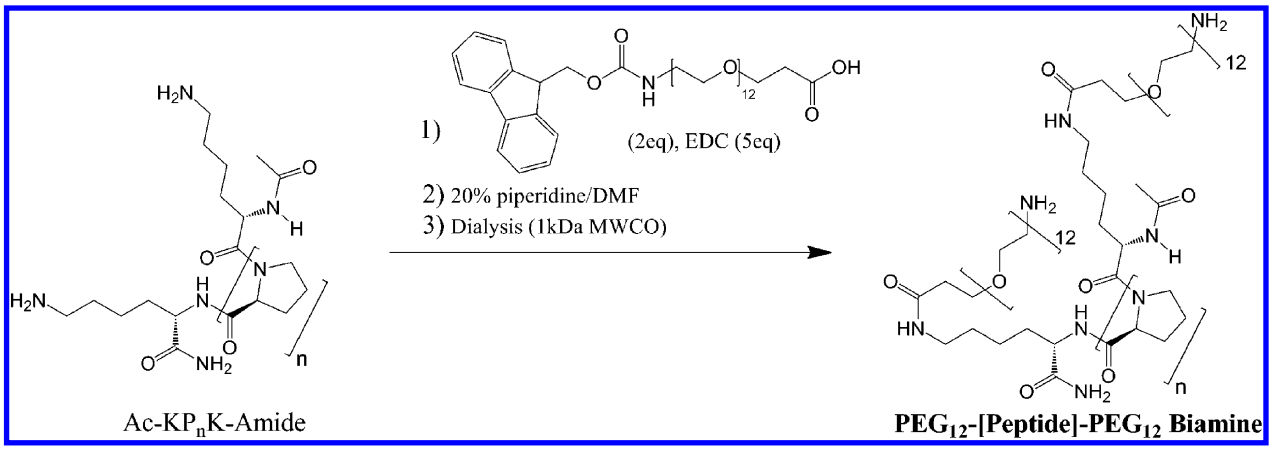

histidine, proline, arginine, and lysine have been found to be particularly susceptible to oxidative processes.[19] Further, the reaction of proline residues with environmental oxidants can lead to cleavage of the parent polypeptide chains at these sites.[20]

Inspired by this work, we synthesized polymeric scaffolds cross-linked with proline oligomers and assessed their degradation following exposure to oxidative environments. As a backbone, we selected a terpolymer system composed of PEG, poly(ε-caprolactone) (PCL), and poly(carboxyl-ε-caprolactone) (cPCL). The selection of this terpolymer system was driven by the functional properties of each component, as the PEG provides hydrophilicity and reduces protein adsorption,[21] the PCL provides elastic mechanical strength and hydrophobicity for cell adhesion,[22] and the cPCL provides carboxylic groups that can be chemically cross-linked with biaminated species under mild conditions. Copolymers of x mol % PEG, y mol % PCL, and z mol % cPCL are identified as x%PEG-b-y% PCL-co-z%cPCL, where PEG-PCL is a block copolymer, but cPCL addition is random within the PCL subunit. This new class of copolymers is designed, providing tunable properties for biomedical applications as polymer properties are influenced by the molar ratios of the individual subunits, and by varying their aforementioned contributions, the resulting physical, chemical, and mechanical properties can be controlled.[23] In particular, the studies below used a 4%PEG-86%PCL-10%cPCL system. PCL was chosen as the majority component because it has been shown to be minimally degraded in environments containing H_2O_2 over more than 20 weeks, requiring much stronger metal-catalyzed oxidative environments to produce any significant degradation within this time frame.[24]

The proline oligomers Ac-KP$_n$K, in which n indicates the number of proline residues, were synthesized by standard Fmoc chemistry on a Rink amide resin to fashion two free amines for the coupling of Fmoc-PEG$_{12}$-COOH (MW = 500 Da). The oxidative degradation of the peptides with and without PEGylation was first assessed through gel permeation chromatography (GPC) and high performance liquid chromatography–mass spectrometry (HPLC-MS). Next, scaffolds of 4%PEG-86%PCL-10%cPCL were covalently cross-linked with PEG-P$_n$-PEG cross-linkers and degraded in acellular and cellular in vitro models mimicking physiologic oxidative conditions. Oxidation-dependent changes in scaffold material properties and morphology were assessed via scanning electron microscopy (SEM), differential scanning calorimetry (DSC), and X-ray microcomputed tomography (μCT) imaging.

EXPERIMENTAL SECTION

Materials. All reagents, including murine γ-interferon (IFNγ) and bacterial lipopolysaccharide (LPS), were purchased from Sigma-Aldrich (St. Louis, MO) and used as purchased unless otherwise noted below. ε-Caprolactone was purchased from Alfa Aesar (Ward Hill, MA). Fmoc-protected L-amino acids and resins for solid-phase peptide synthesis were purchased from EMD Biosciences (Gibbstown, NJ). RPMI-1640 medium, penicillin–streptomycin, and fetal bovine serum (FBS) were purchased from Invitrogen (Carlsbad, CA). 3-Morpholinosydnonimine (SIN-1) was purchased from Invitrogen as packages of individual 1 mg aliquots. Dialysis filters were purchased from Thermo Fisher (Rockford, IL). All organic solvents, including N,N-dimethylformamide (DMF), N-methylpyrrolidone (NMP), tetrahydrofuran (THF), and methanol, were purchased from Fisher Scientific (Pittsburgh, PA) and used as purchased.

The ring-opening polymerization of ε-caprolactone is highly water-sensitive, and therefore, all monomers and reagents for this purpose were carefully dried before use. A total of 15 g MeO-PEG (M_n = 5000 Da; ~3 mmol) was dissolved in 150 mL of toluene and dried via a Dean–Stark trap at 130 °C under N_2 environment. The dried MeO-PEG was concentrated by distillation at 40° C, precipitated in diethyl ether at −20 °C, then further dried in vacuo. In a separate vessel, 150 mL of ε-caprolactone (161.7 g; 1.41 mol) was mixed with 2 g calcium hydride (47.5 mmol) overnight under N_2 gas. The product was distilled in vacuo at 70 °C, and stored under N_2 until use.

Synthesis of Biaminated PEG-P$_n$-PEG "Cross-Linkers". The peptide sequences KPPPPPK (P_5), KPPPPPPPK (P_7), and KPPPPPPPPPPK (P_{10}) were synthesized via standard Fmoc-based solid phase methods on a Rink amide-MBHA resin (Scheme 1). The peptides were then acetylated in excess acetic anhydride for 4 h, prior to cleavage in a 95:5:3:2 mixture of trifluoroacetic acid/thioanisole/ethanedithiol/anisole for 2 h. The liberated peptide was precipitated in diethyl ether and lyophilized to form a dense, white powder. All peptides were at least 70% acetylated as determined by HPLC-MS, therefore, containing only two amine groups for downstream coupling, which are located on the lysine residues. As a result of incomplete acetylation of the peptides, the remaining <30% of peptide also contained a third amine group responsible for the N-terminus of the peptide chain.

Fmoc-PEG$_{12}$-COOH (EMD Biosciences) was then coupled to the peptides via standard carbodiimide chemistry.[25] Removal of the Fmoc-protecting group was achieved via 20% piperidine in DMF, followed by dialysis of the completed cross-linkers in 1 kDa MWCO membranes for 48 h against nanopure water. Lyophilization of the retentate yielded a white, fluffy powder that was stored at −20 °C until use.

Scheme 2. Synthesis of *x*%PEG-*y*%PCL-*z*%cPCL Backbone Polymers

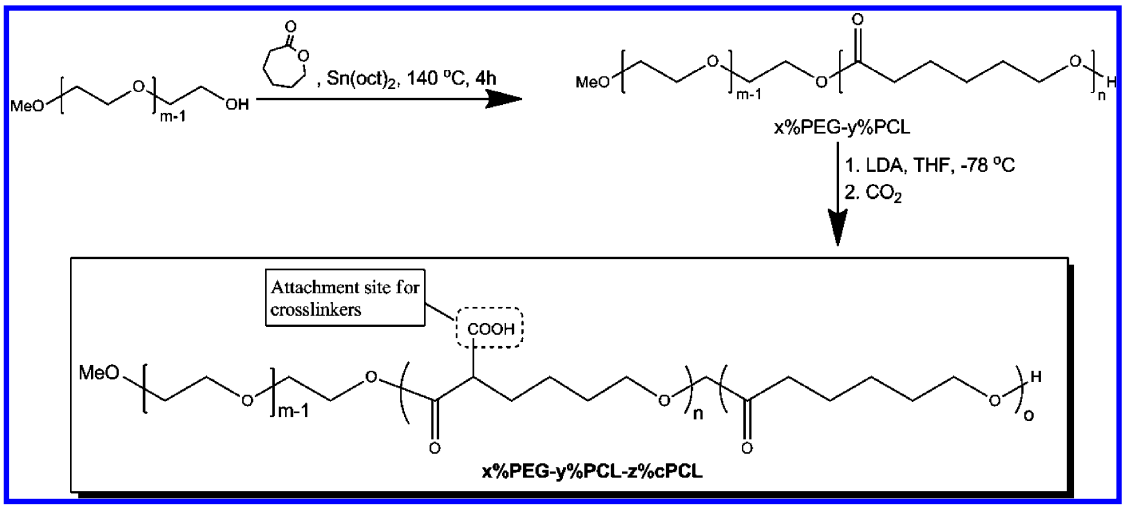

Synthesis of 4%PEG-86%PCL-10%cPCL "Backbone" Polymers. To synthesize *x*%PEG-*y*%PCL block copolymers (Scheme 2), 0.4 g dried MeO-PEG (0.08 mmol) was added to a round-bottom flask. The flask was capped with septum, heated to 40 °C, and degassed with repeated cycles of evacuation followed by equilibration with N_2. Next, 9.4 g ε-caprolactone (82 mmol) and 17.9 mg of tin 2-ethylhexanoate (44.2 μmol) in 500 μL of toluene were injected sequentially into the reaction vessel. The polymerization was carried out at 140 °C for 4 h. The resultant 100 kDa 4%PEG-96%PCL was cooled to room temperature, dissolved in 200 mL methylene chloride, precipitated in diethyl ether, and dried in vacuo.

The formation of *x*%PEG-*y*%PCL-*z*%cPCL was carried out via random carboxylation of the *x*%PEG-*y*%PCL diblock copolymers. A total of 8.57 g of 4%PEG-96%PCL was evacuated in a round-bottom flask for 1 h and then dissolved in 300 mL of anhydrous THF. The solution was cooled to −78 °C and 37.5 mL of 2 M lithium diisopropylamide (LDA; 75 mmol) was injected dropwise by syringe. This reaction proceeded for 30 min at −78 °C. In a separate Schlenk flask, CO_2 was generated through the reaction of concentrated sulfuric acid with sodium carbonate and dried through a column filled with molecular sieves and sodium hydride. The resulting dry CO_2 was bubbled through the 4%PEG-96%PCL/LDA reaction for 30 min at −78 °C, during which the reaction exhibits a color change from orange to white. The solution was then brought to room temperature, and 150 mL of 1 M ammonium chloride was added dropwise. The solution was then neutralized by dropwise addition of hydrochloric acid. The crude product was extracted with 500 mL of methylene chloride, and the pooled organic fractions were concentrated via rotary evaporation. 4%PEG-86%PCL-10%CPCL was precipitated in diethyl ether and dried in vacuo. ^{1}H NMR (400 MHz; $CDCl_3$): δ 9.25 (s, <1 H, COO**H**), 4.06 (t, 2H, -OC**H**$_2$), 3.4 (m, 1H, -C**H**-COOH), 2.31 (t, 2H, -C**H**$_2$), 1.66 (m, 4H, -C**H**$_2$), 1.5 (m, 2H, -C**H**$_2$), 1.37 (m, 2H, -C**H**$_2$).

Scaffold Fabrication. A total of 0.3 g of the 4%PEG-86%PCL-10%cPCL terpolymers were dissolved in 3 mL of ice cold CH_2Cl_2 and was followed by the addition of 67 mg of cross-linkers and 12 mg of *N*-ethyl-*N*′-(3-dimethylaminopropyl) carbodiimide hydrochloride (EDC). For control scaffolds, 2 kDa PEG-dihydrazide (Laysan Bio, Arab, AL) was used in place of the PEG-P_n-PEG cross-linkers. After vortexing this mixture vigorously, the solution was poured into a Teflon dish 5 cm in diameter, containing 10 g of presieved NaCl crystals (212−425 μm). This mixture was manually mixed vigorously to spread the salt crystals evenly throughout the prepolymer, and then the prepolymer was evenly spread throughout the bottom of the Teflon dish. The prepolymer was allowed to cross-link over ice for 30 min. Next, the polymers were immersed in liquid N_2 for 2 min and lyophilized overnight to remove all traces of organic solvents. The removal of excess byproducts, salts, and reagents was achieved by salt-leaching the scaffolds in nanopure water over 5 days. Water was changed daily. Finally, the completed scaffolds were dried in vacuo overnight at room temperature, and weighed prior to use in any experiments. Wet masses of the scaffolds was measured after allowing scaffolds 3 days to swell to equilibrium. Swollen scaffolds were blotted dry to remove excess buffer before weighing. Swelling ratio was calculated according to the formula [swelling ratio] = (wet mass)/(dry mass).

Oxidation Experiments and Chromatography. To investigate oxidative degradation, peptide cross-linkers were incubated in 1 mg/mL in phosphate-buffered saline (PBS, pH 7.4) at 37 °C, and then H_2O_2 and $CuSO_4$ were added to the samples to final concentrations of 5 mM H_2O_2 and 50 μM Cu(II). Peptide cross-linkers that were incubated in the absence of H_2O_2 and $CuSO_4$ served as a control. Reactions were incubated in the dark at 37 °C until they were ready for analysis, at which point they were frozen at −20 °C, effectively stopping the oxidation reaction.

For scaffold degradation experiments, dry scaffolds were weighed before incubation then allowed 3 days to swell to equilibrium in PBS prior to the beginning of the experiment. From here, scaffolds were incubated in PBS with or without 1 mM SIN-1 for 28 days. Buffers were changed daily owing to the relatively short half-life of SIN-1 in aqueous environments (<10 h). At days 3, 7, 14, and 28 post incubation, scaffolds were dried in vacuo overnight prior to reweighing and further characterization.

GPC was performed by injecting samples into three serial Tosoh Biosciences TSKGel Alpha columns (Tokyo, Japan), operated at 60 °C. For various experiments, water or DMF with 0.1 M LiBr were used as mobile phases. Chromatograms were recorded via a Shimadzu SPD-10A UV detector and RID-10A refractive index detector (Shimadzu Scientific Instruments, Columbia, MD), and a Wyatt miniDAWN Treos multiangle light scattering detector (MALS; Wyatt Technology, Santa Barbara, CA). Data acquisition and analysis was performed on Wyatt ASTRA software (version 5.3.4).

Analytical high performance liquid chromatography−mass spectrometry (HPLC-MS) was performed on an Agilent 1200 series system equipped with UV detection at 215 and 254 nm and a 6130 quadrupole mass spectrometer with electrospray ionization (Agilent Technologies, Santa Clara, CA). Online evaporative light-scattering detection was also activated for some samples (Varian, Santa Clara, CA). C18 columns were purchased from Phenomenex (Kinetex 2.1 × 5.0 mm; Torrance, CA), and run with a gradient of 10−95% acetonitrile (over 2 min) in 0.1% trifluoroacetic acid in water.

Scanning Electron Microscopy (SEM). SEM was performed on a Hitachi S-4200 system (Tokyo, Japan). An accelerating voltage of 2 kV was used for all images. To prepare scaffolds for imaging, scaffolds were sputter-coated with gold (Cressington Sputter Coater 108, Watford, United Kingdom) at a plasma current of 30 mA for 120 s.

dx.doi.org/10.1021/bm201328k | *Biomacromolecules* 2011, 12, 4357−4366

Differential Scanning Calorimetry (DSC). All polymeric scaffolds were analyzed for thermal transitions and heat capacity via DSC (TA Instruments, Newcastle, DE). Samples were weighed (2−5 mg), and sealed within aluminum sample pans with tops. The measurement procedure included two temperature sweeps from −80 to 100 °C at a ramp rate of 10 °C/min. The values from the second sweep were reported such that thermal history was erased.

Cell Studies. For cell studies, immortalized bone-marrow-derived macrophages (BMDMs) were generated from NGL (NF-κB-GFP-Luciferase construct) transgenic mouse lines on C57Bl6/DBA background (NGL-BMDMs), and were provided by the laboratory of Dr. Fiona E. Yull (Vanderbilt-Ingram Cancer Center, Nashville, TN).[26] NGL-BMDMs were grown in high-glucose (4.5 g/L) DMEM containing 4 mM L-glutamine and further supplemented with 10% (v/v) FBS and 1% (v/v) penicillin−streptomycin. All cells were cultured at 37 °C in a 5% CO_2 incubator.

For all experiments, NGL-BMDMs were detached from flasks by gently rinsing the confluent monolayers with serum-free medium (high-glucose DMEM with 4 mM L-glutamine, 1% penicillin−streptomycin, 1× nonessential amino acids, and 1× MEM vitamins), counted via a Coulter Counter (Beckman Coulter, Miami, FL) and seeded into scaffolds or directly to 24-well plates at a density of 300000 cells/cm^2. Cells were allowed 24 h to associate with scaffolds or well plates before further experimentation. The serum-free medium was used in the course of the experiment to minimize serum-induced changes in macrophage activation states.

For pro-inflammatory activation, NGL-BMDMs were treated with 50 ng/mL IFNγ and 10 μg/mL LPS in serum-free medium. To maintain a high level of macrophage activation, media containing these activators was replaced daily for the duration of the experiments.

Microcomputed Tomography (μCT) Imaging of Scaffolds. To analyze the porosity and the distribution of pore size in the scaffolds, portions of each scaffold were imaged using a μCT50 (Scanco Medical, AG, Switzerland) and the manufacturer's software. Images of an approximately 6 mm wide by 10 mm long section of each sample were acquired with an isotropic voxel size of 1 μm at 45 kV, 200 μA, 1000 projections per rotation, and an integration time of 1 s without beam filtering and using the default beam hardening correction. Three different scaffolds were imaged per experimental condition (n = 3). The low X-ray attenuation of the scaffolds was offset by the extremely low noise produced by the extended acquisition protocol which maintained signal-to-noise ratio sufficient for threshold based segmentation of scaffold from internal pores. A cylinder of 1355 μm in diameter and 500 μm long was selected as the volume of interest in each sample. After creating a z-stack of the individual slices, the volume of interest (VOI) was extracted and the threshold and noise filter applied to extract the 3D pore structure from the gray scale images. The mean pore diameter and distribution of the pore diameters within each scaffold was calculated using standard, accepted ball filling method reported elsewhere.[27,28] By distance transformation, the calculation of the metric distance of every pore voxel to the nearest pore-matrix interface is understood. These distances can be imagined as the radius of a sphere with center in this voxel that fits inside the pore. Redundant spheres are removed such that big spheres incorporate small, encompassed spheres. The result is the midaxes transformed structure with the centers of maximal spheres filling the pore completely. To calculate pore thickness, each voxel then gets the value of the radius of the maximal sphere it sits within.

RESULTS

Synthesis and Characterization of PEG-P$_n$-PEG Cross-Linkers and 4%PEG-86%PCL-10%cPCL Backbone. The two major components of the scaffolds were synthesized via well-characterized methods, as described, and characterized by GPC (Figure 1). The cross-linkers primarily consisted of bi-PEGylated proline oligomers, as evidenced by the predominant peak at 29.5 min, but also included smaller amounts of tri-PEGylated proline oligomers, as indicated by the earlier-eluting peak between 26 and 27 min. The presence of this minor peak is due to incomplete acetylation of the peptide prior to coupling of the PEG sequences. Nevertheless, all three cross-linker sequences exhibited similar sizes, as indicated by their overlapping chromatograms.

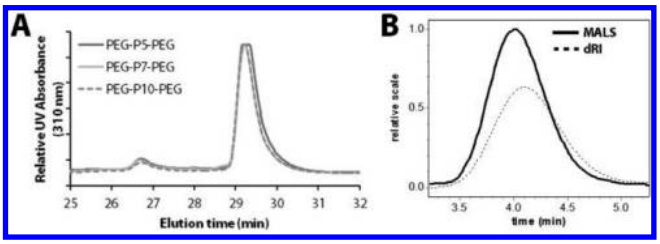

Figure 1. GPC chromatograms of the synthesized scaffold components. (A) PEG-P$_n$-PEG cross-linkers (10 mg/mL in DMF + 0.1 M LiBr) prior to final Fmoc deprotection are detectable via a UV detector set at 310 nm. The presence of a small, earlier-eluting hump at ∼27 min represents the tri-PEGylated peptides due to incomplete acetylation of the peptide sequences. The major peak at 29−30 min is the major, bi-PEGylated product. (B) The 4%PEG-86%PCL-10% cPCL backbone (10 mg/mL in THF) is relatively monodisperse, as evidenced by the near-complete overlap of the MALS and differential refractive index (dRI) chromatograms. With the dn/dc of the terpolymer measured at 0.0663 mL/g in THF, the molecular weights were calculated at M_n = 99.4 kDa and M_w = 115 kDa (PDI = 1.16).

The terpolymer backbone was synthesized via the polymerization of ε-caprolactone onto a PEG-based macroinitiator, followed by random carboxylation of the PCL block.[29] This scheme led to a relatively monodisperse terpolymer of M_n = 99.4 kDa and M_w = 115 kDa (PDI = 1.16), as measured via GPC-MALS. The terpolymer exhibited a dn/dc of 0.0663 mL/g in THF and was poorly soluble in methanol, DMF, and N-methylpyrolidone, characteristics that are consistent with the primarily PCL composition of the terpolymer.[30]

H_2O_2-Mediated Degradation of P$_n$ Peptides and PEG-P$_n$-PEG Cross-Linkers. The susceptibility of the peptide components to oxidative cleavage was validated at multiple intermediate steps in the scaffold synthesis, starting from the completed peptides. In this way, the oxidation-responsiveness of the scaffolds can be attributed primarily to the peptide components and not any other polymeric components.

To begin, as-synthesized proline oligomers were incubated in PBS at 37 °C, with or without the mediators of metal-catalyzed oxidation (MCO). The samples were then analyzed by HPLC-MS to detect the presence of peptides and degradation byproducts (Figure 2). In particular, after a four day incubation in the MCO environment, the P_{10} oligomers demonstrated significant changes in their UV chromatogram within the elution time regions specific for the intact peptide, as well as the concomitant disappearance of MS peaks at 1244 and 623 m/z that are characteristic of the intact peptide. These phenomena were not observed for reactions that were incubated at room temperature for the same time period (data not shown), indicating that physiological temperature is required to induce the oxidative cleavage of peptides.

To confirm the oxidation-induced cleavage of the peptides, the PEG-P$_n$-PEG cross-linkers were incubated under the same conditions, and analyzed by GPC. In all cases, MCO-treated cross-linkers eluted later than untreated cross-linkers, indicating a decrease in the hydrodynamic size of these cross-linkers following oxidative treatment. Further, the average molecular weights of the cross-linkers were calculated relative to

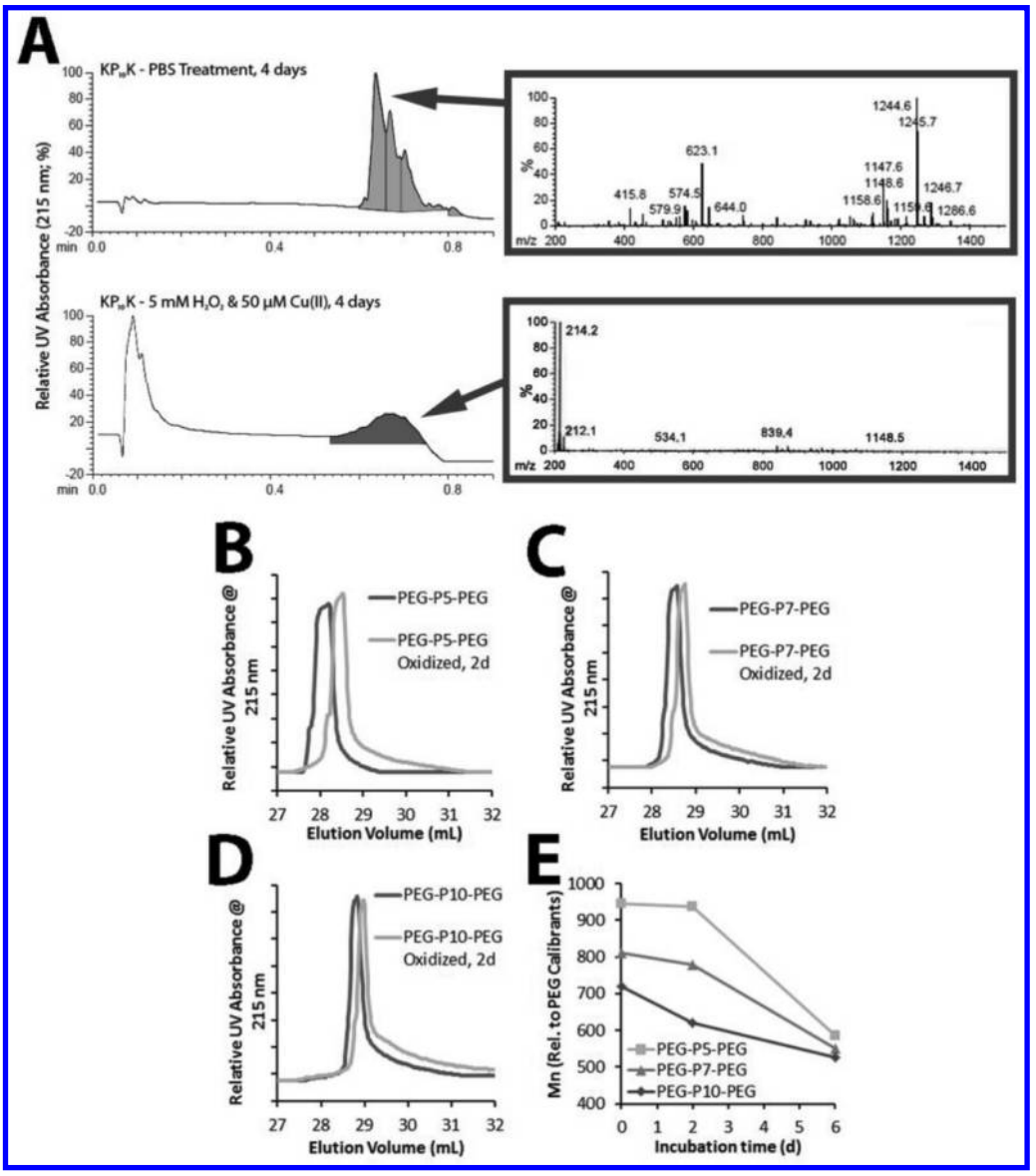

Figure 2. Metal-catalyzed oxidation of proline oligomers. (A) P_{10} was incubated at 37 °C for 4 days in PBS only or PBS containing H_2O_2 and Cu(II) and then analyzed via HPLC-MS. The latter treatment resulted in the disappearance of chromatograms and mass spectra characteristic of the intact peptide. To further confirm oxidative degradation of the peptide, PEG-P_n-PEG was incubated under the same conditions prior to analysis via GPC (B–E). In all cases, these molecules eluted at later times following only 2 d in the oxidative environment. (E) Peak molecular weights were calculated based on elution time, relative to monodisperse PEG standards. Within the first 2 d of treatment, the degradation rate was proportional to the length of the proline oligomers. Further, all cross-linkers degraded to form a 550 Da product within 6 d, which is consistent with the molecular weight of the PEG reagent that was coupled to both ends of the peptides used in the study, to form the PEG-P_n-PEG cross-linkers for the scaffolds.

monodisperse PEG standards, and within the first two days of MCO treatment, the degradation rate of the cross-linkers was proportional to the length of the proline oligomers contained within the cross-linkers. Moreover, after six days of MCO treatment, the molecular weights of the different cross-linkers converged on 550 Da, the molecular weight of the PEG component flanking each end of the peptides, indicating the complete degradation of the proline component of the cross-linkers.

Fabrication and Characterization of Cross-Linked 4% PEG-86%PCL-10%cPCL Terpolymer Scaffolds. Polymeric scaffolds exhibiting macroporous and microporous architecture were fabricated using a procedure adapted from previous methods.[31] The completed scaffolds were morphologically examined via SEM (Figure 3). By dissolving the prepolymer mixture in a hydrophobic solvent, the condensation of water due to the amine–carboxylic acid cross-linking reaction results in the phase separation of water from the bulk solvent, producing micropores (diameter < 10 μm) in the polymer network. Macropores of >100 μm in diameter were templated into the polymer network by performing this cross-linking reaction in a bed of presieved NaCl salt crystals. While all scaffold types appeared morphologically similar, PEG-dihydrazide cross-linked scaffolds produced noticeably fewer micropores.

To examine if this was due in part to the hygroscopic nature of PEG-dihydrazide, swelling ratios of the scaffolds were measured as a function of the cross-linker employed. Due to the primarily PCL composition of the polymers, the resulting scaffolds exhibited swelling ratios that were on the order of 10×

dx.doi.org/10.1021/bm201328k | Biomacromolecules 2011, 12, 4357–4366

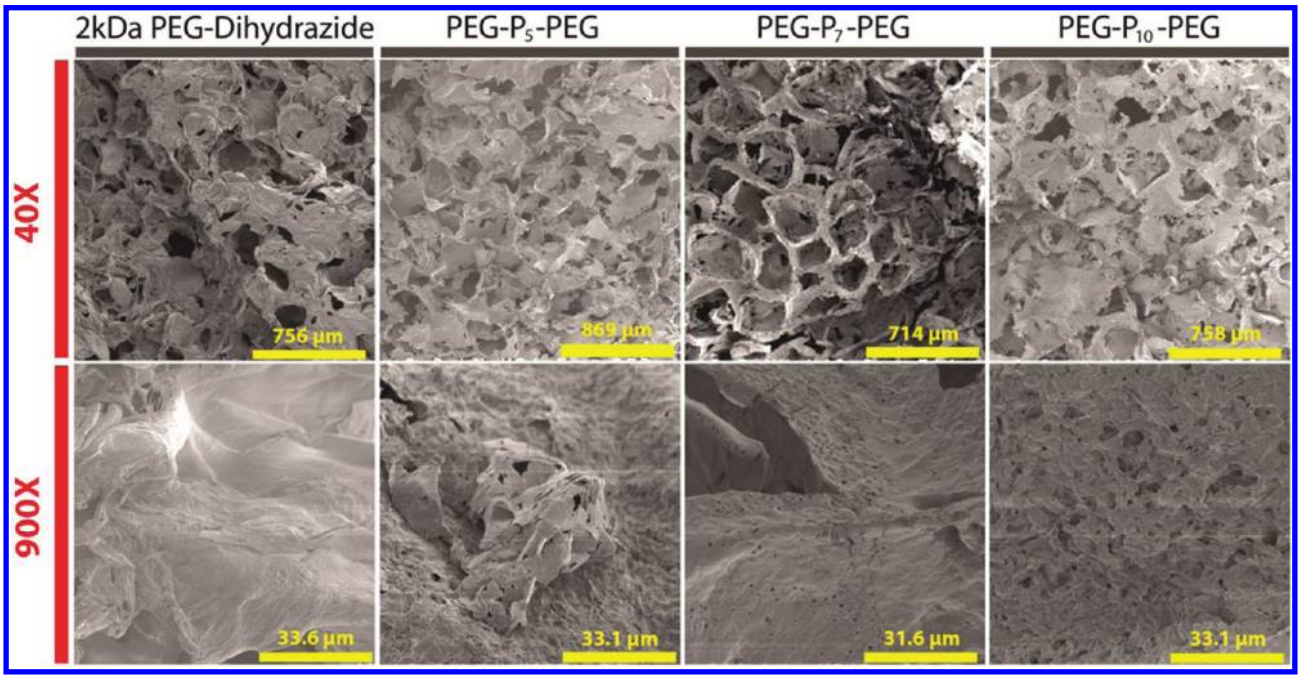

Figure 3. SEM images of the scaffolds of 4%PEG-86%PCL-10%cPCL by cross-linker type. Two different magnifications showcase macropores of >100 μm diameter (top row) and micropores of <10 μm in diameter (bottom row). Only the PEG-dihydrazide-cross-linked scaffolds failed to show any widespread microporous architecture. Macropores were templated into the polymer network through a salt-leaching procedure, while micropores were generated through the phase separation of the water generated during the cross-linking reaction from the hydrophobic solvent used to dissolve the prepolymer.

lower than those typically exhibited by hydrogels (Figure 4). However, the swelling ratios can be controlled to some extent

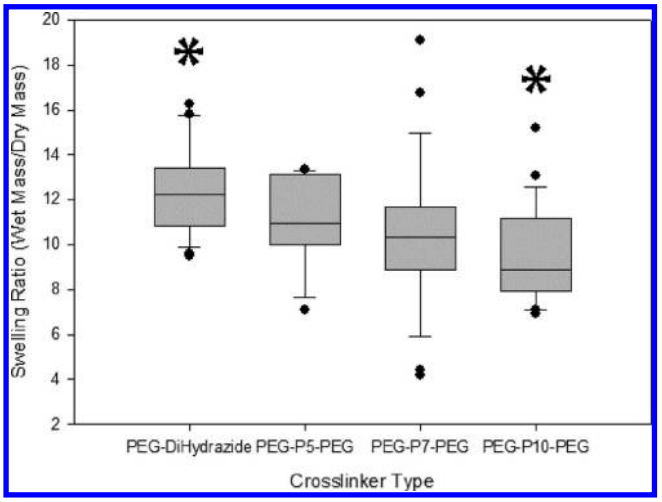

Figure 4. Box-and-whisker plots representing swelling ratios of 4% PEG-86%PCL-10%cPCL scaffolds by cross-linker type. Upper and lower ends of boxes represent the 25th and 75th percentiles, respectively. Solid lines represent the median swelling ratios. Whiskers indicate 90th and 10th percentiles, and dots indicate outliers. The ability of the scaffolds to retain water was somewhat related to the length of the proline oligomer used as a cross-linker. PEG-P_{10}-PEG cross-linked scaffolds retained significantly less water than PEG-dihydrazide cross-linked scaffolds ($*p < 0.05$, $n = 24$). Differences in swelling ratios vs the other two scaffold types were not statistically significant.

by varying the length of the oligo(proline) peptide used in the cross-linker. PEG-dihydrazide, PEG-P_5-PEG, PEG-P_7-PEG, and PEG-P_{10}-PEG cross-linked scaffolds exhibited swelling ratios of 12.4 ± 1.9 ($n = 24$), 11.1 ± 1.9 ($n = 12$), 10.4 ± 3.2 ($n = 24$), and 9.5 ± 2.1 ($n = 24$), respectively. Across these four groups, only PEG-dihydrazide versus PEG-P_{10}-PEG exhibited statistically significant differences in hydration ($p < 0.05$).

We also attempted the fabrication of the scaffolds using other solvents to dissolve the prepolymer, including *N*-methylpyrrolidone (NMP), THF, and toluene. When NMP is used, the resulting scaffolds completely disintegrate into small clumps during the salt-leaching process. This is consistent with the poor solubility of PCL in NMP and suggests that widespread cross-linked polymer networks were not successfully formed under these conditions. Toluene and THF both solubilized the prepolymer, and produced cross-linked, macroporous scaffolds following salt-leaching. However, examination of these scaffolds via SEM failed to show any micropores in the resulting polymer network.

Overall, these results suggest the successful formulation of widespread cross-linked polymeric scaffolds of relatively uniform macroporous and microporous architecture, via the methods described above. The scaffolds are also capable of absorbing about 10-fold their dry mass in water.

ROS-Mediated Oxidative Degradation of Cross-Linked Scaffolds. Because control PEG-dihydrazide cross-linked scaffolds and PEG-P_7-PEG cross-linked scaffolds demonstrated similar morphology (Figure 3) and an insignificant difference in swelling ratios, these two scaffold types were selected for further study. To verify that the proline cross-linkers can accelerate the degradation of the scaffolds under oxidative conditions, scaffolds were soaked for up to 28 d at 37 °C in buffer with or without 1 mM of the ROS generator SIN-1. SIN-1 is typically known to produce nitric oxide and superoxide simultaneously, which can further lead to the generation of peroxynitrite and hydroxyl radicals in situ.[32] At each time point, scaffolds were dried and weighed.

Whereas the dry mass of scaffolds soaked in PBS only did not change significantly over the 28 d incubation period, both scaffold types underwent significant degradation within the oxidative environment (Figure 5). Under oxidative conditions,

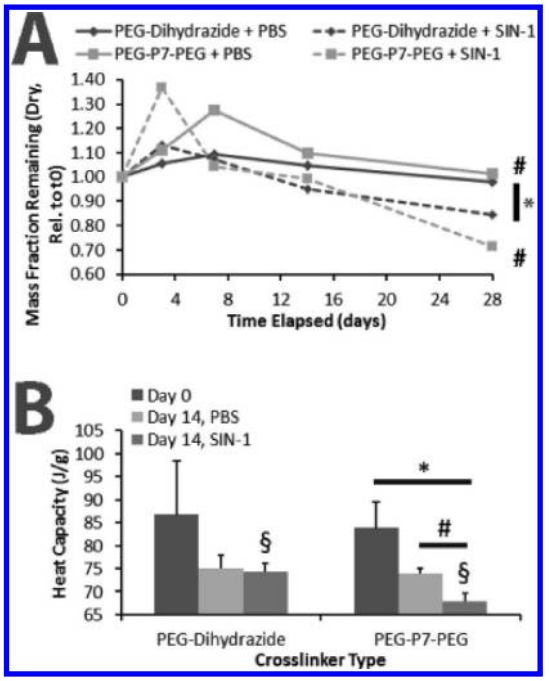

Figure 5. Accelerated degradation of terpolymer scaffolds cross-linked with PEG-P_7-PEG cross-linkers. Scaffolds cross-linked with PEG-dihydrazide or PEG-P_7-PEG were soaked in PBS or PBS + 1 mM SIN-1 for 28 days. (A) At each time point, scaffolds were dried and massed. The average remaining mass fraction of each scaffold is calculated by dividing dry mass following treatment by dry mass at the beginning of the study. Scaffolds containing both cross-linker types experienced some degree of oxidative degradation, but PEG-P_7-PEG cross-linked scaffolds lost more mass under oxidative conditions ($^{\#}$,$^{*}p < 0.05$, $n = 3$). (B) Heat capacity of scaffolds for the melting point transition following a 14 d treatment was measured via DSC. Error bars represent the standard deviation of three independent experiments ($^{\#}p < 0.01$, $n = 3$; $^{*}p < 0.05$; $^{\S}p < 0.05$).

PEG-dihydrazide cross-linked scaffolds retained 85 ± 5% of their mass following 28 d of treatment, while PEG-P_7-PEG cross-linked scaffolds retained 72 ± 18% of their mass ($n = 3$). Neither scaffold completely degraded in this time frame. This can be attributed to the composition of the scaffolds, which is ~82% terpolymer by weight.

The oxidative degradation of both scaffold types was further characterized by DSC. These results showed that all scaffolds exhibited melting points at 53−56 °C regardless of treatment duration and type or cross-linker. However, the oxidative degradation of the PEG-P_7-PEG scaffolds resulted in significantly decreased heat capacities during this phase transition (67.8 ± 1.8 J/g, $n = 3$), relative to PBS-only treated scaffolds (73.8 ± 1.2 J/g). This difference was not seen for the correspondingly treated PEG-dihydrazide cross-linked scaffolds (75.0 ± 3.0 J/g in PBS vs 74.4 ± 1.6 J/g in SIN-1). Further, following 14 d of treatment with SIN-1 in PBS, all scaffolds exhibited significantly lower heat capacities, as compared to their day 0, untreated counterparts. This phenomenon is attributable to hydrolysis of the polymer networks, which can occur throughout the incubation period.

Macrophage-Mediated Oxidative Degradation of Cross-Linked Scaffolds. To evaluate the oxidative degradation of the scaffolds in a cellular model of oxidative stress, immortalized murine BMDMs were cultured on the scaffolds for 9 d with or without pro-inflammatory activation using 50 ng/mL IFNγ and 10 μg/mL LPS. This model was used because macrophages primed with γ-interferon (IFNγ) and activated with LPS typically respond through the upregulation of the M1, pro-inflammatory phenotype, which results in increased production of ROS and nitric oxide.[33] When cultured in tissue culture plates, the immortalized BMDMs produced higher

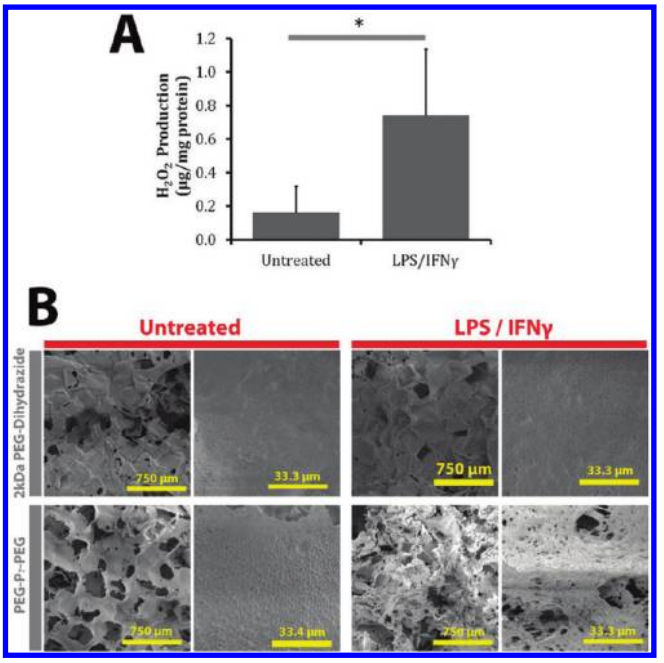

Figure 6. LPS/IFNγ-activated BMDMs exhibited H_2O_2-dependent degradation of PEG-P_7-PEG-cross-linked scaffolds. (A) Immortalized murine BMDMs cultured in tissue culture plates for 24 h in the presence of 50 ng/mL IFNγ and 10 μg/mL LPS produced higher levels of H_2O_2 per cell (H_2O_2 production normalized to cell number indirectly via protein assay), relative to untreated BMDMs ($^{*}p < 0.05$, $n = 3$). (B) SEM images (40× and 900×) of scaffolds incubated with untreated or activated BMDMs for 9 d. Only PEG-P_7-PEG cross-linked scaffolds incubated with activated BMDMs exhibited the appearance of widespread pitting and <10 μm pores in the polymer network.

levels of H_2O_2 per cell, relative to untreated BMDMs (Figure 6A).

The increased peroxide production by the immortalized BMDMs due to IFNγ/LPS treatment likely facilitated the accelerated degradation of PEG-P_7-PEG cross-linked scaffolds (Figure 6B). This was evidenced by the appearance of widespread pitting and <10 μm pores in the polymer networks of peptide-containing scaffolds incubated in the presence of activated BMDMs. For all scaffolds that were incubated with nonactivated BMDMs, as well as PEG-dihydrazide cross-linked scaffolds treated with activated BMDMs, the scaffolds exhibited no observable changes in pore architecture during the same incubation period.

To quantify these changes in the pore architecture of the scaffolds, scaffolds were imaged via μCT, and the porosity was assessed from the reconstructed images (Figure 7). 3D heat

dx.doi.org/10.1021/bm201328k | Biomacromolecules 2011, 12, 4357−4366

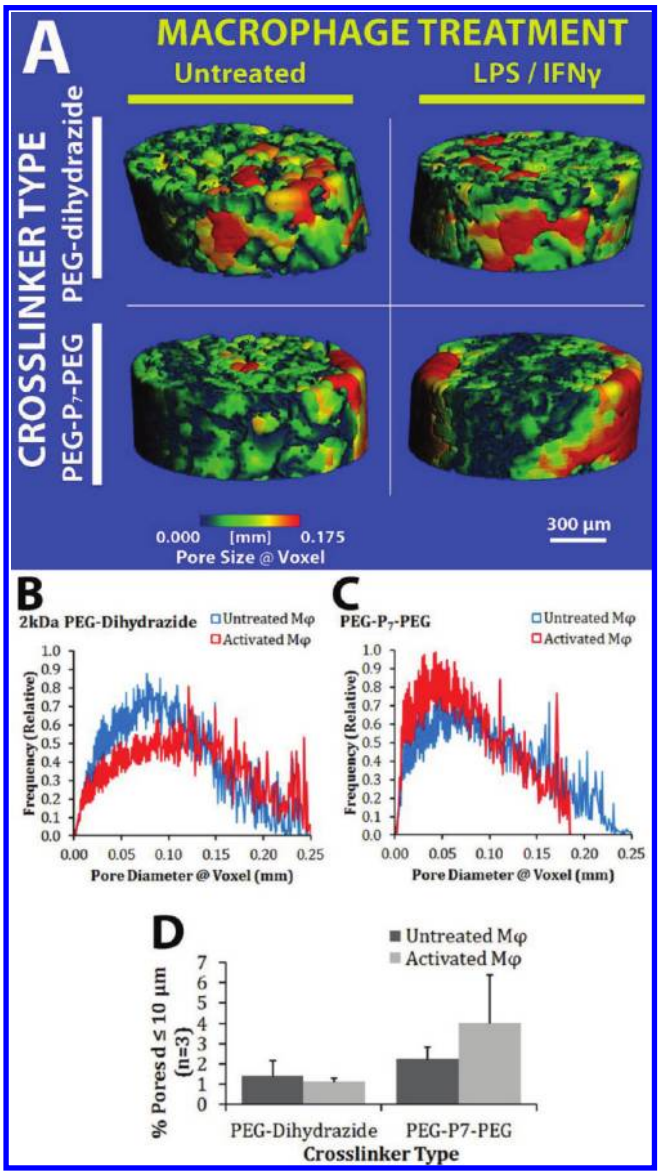

Figure 7. μCT imaging of scaffolds incubated with NGL-BMDMs (Mφ). Isotropic voxel size = 1 μm. (A) 3D pore diameter heat maps of scaffolds following incubation with untreated or activated (LPS/IFNγ-treated) BMDMs for 9 d. (B–C) Pore diameter histograms for scaffolds by cross-linker and treatment (average of n = 3 independent experiments). (D) From these histograms, a range of pore diameters (0–10 μm) was gated as an ROI, and the cumulative percentage of voxels containing pores of diameters within this range was plotted vs cross-linker type and treatment method. Consistent with the intended drug delivery function of this scaffold, the PEG-P_7-PEG cross-linked scaffolds experienced an increase in the appearance of small pores ≤10 μm in diameter. These results are consistent with SEM observations demonstrating the appearance of micropores and pits in these polymer matrices as well as the widespread disintegration of the macroporous scaffold structure, as shown in (A).

maps of the pore sizes at each voxel were constructed, and pores were visualized as the blue regions in the images (Figure 7A). Notably, macropores were evident in all nondegraded scaffolds. However, the PEG-P_7-PEG cross-linked scaffolds seeded with activated BMDMs exhibited a high density of blue voxels, indicating the increased occurrence of micropores in this scaffold (Figure 7A). These observations are consistent with observations via SEM (Figure 6).

The distribution of pore diameters was plotted from these images. PEG-dihydrazide cross-linked scaffolds exhibited similar pore size distributions regardless of whether they were incubated with untreated or activated BMDMs (Figure 7B). However, in PEG-P_7-PEG cross-linked scaffolds, activated BMDMs elevated the presence of micropores (diameters < 10 μm; Figure 7C). Because SEM results showed an increase in the occurrence of pores with diameters <10 μm within these particular scaffolds, the 0–10 μm pore diameter range was gated as a region of interest (ROI), and the number of voxels that contain pores within this range can be measured as a percentage of the total number of voxels in the 3D image. After incubation with untreated BMDMs for 9 d, 1.4 ± 0.7% and 2.2 ± 0.6% of pores within PEG-dihydrazide and PEG-P_7-PEG cross-linked scaffolds, respectively, were generated within the ROI. PEG-dihydrazide cross-linked scaffolds incubated with activated BMDMs for the same time period contained 1.1 ± 0.2% pores within the ROI. PEG-P_7-PEG cross-linked scaffolds under these same conditions demonstrated a noticeable increase in pores within the ROI (4.0 ± 2.4%) relative to the same scaffold type incubated with untreated BMDMs.

DISCUSSION

The goal of the present work is to demonstrate proof-of-concept of ROS-mediated degradable scaffolds through the covalent association of ROS-responsive cross-linkers with nonresponsive backbone polymers. Such a scaffold provides a new model in the toolbox to design an ROS-responsive biomaterials platform that exerts effects over a much longer time scale than the poly(propylene sulfide)-based platform.[13]

Proline oligomers were selected to be the ROS-responsive component of the model scaffold, based on earlier work by Amici et al., which demonstrated that proline, histidine, lysine, and arginine residues within polypeptide chains are particularly susceptible to oxidative cleavage.[19] While oligomers of these other amino acids were not investigated as cross-linkers in the work presented here, they are expected to also be degradable under oxidative environments. Nevertheless, proline oligomers were selected in this study because proline is the only naturally occurring amino acid that is capable of forming a tertiary amide bond, which is known to be more easily oxidized than secondary amide bonds.[34] It is therefore expected that linear peptide or polymer chains containing secondary amide linkages can also degrade under oxidative conditions, although the degradation rate may be slower than that of the proline oligomers shown here. The oxidative degradation of the polymer networks containing secondary amide bonds was evidenced by our data, where control PEG-dihydrazide cross-linked scaffolds also experienced degradation through 28 d in 1 mM SIN-1, although not to the same extent as the P_7-cross-linked scaffolds (Figure 5).

With the intended controlled release application of these scaffolds, methods to increase the surface area of contact between the scaffold and the fluid environment were of paramount importance. To achieve this goal, a salt-leaching process was employed in order to introduce pores throughout the cross-linked polymer network. Further, the cross-linking reaction takes place in a hydrophobic solvent. Hence, the condensation of water due to the amine–carboxylic acid cross-linking reaction results in the phase separation of water from the bulk solvent, producing smaller diameter "micropores" (diameter < 10 μm) in the polymer network (Figure 3). The presence of micropores further increases the surface area of

contact between the scaffolds and their environments, but μCT of the scaffolds suggests that micropores account for less than 1% of all the pores in the scaffolds following synthesis. However, following oxidative degradation of the PEG-P_7-PEG cross-linked scaffolds, an increase in the occurrence of these micropores was observed (Figure 7C).

It is also notable that the observed response rates for the polymeric scaffolds in this study are much slower than those observed for other oxidation-responsive scaffolds. For example, poly(propylene sulfide)-based systems have been shown to degrade within the time scale of <6 h in response to H_2O_2.[13] More recently, polythioether ketal nanoparticles were shown to degrade in response to ROS on the order of 15 h, but required an acidic environment to completely degrade.[35] Therefore, the complete degradation of the polymeric system discussed in the current study is expected to occur in >10× as much time as other, alternative systems.

To completely isolate oxidation-responsive behavior to the cross-linkers, alternative coupling chemistries may be necessary to covalently bind the cross-linkers to the backbone polymers. The Huisgen 1,3-dipolar cycloaddition reaction, better known as azide−alkyne "click" chemistry, has been suggested to form linkages that remain relatively inert under oxidative conditions.[36] Alternatively, disulfide bridges are not susceptible to oxidative cleavage, as such conditions actually promote the formation of these "cross-links", even under physiologically relevant constraints.[37] This strategy has been successfully employed by others to form highly cross-linked hydrogels.[38] With the goals and scope of the present work in mind, these modifications are an appropriate subject for further development and refinement of our system.

Nevertheless, the oxidation response of the proline oligomers was tracked throughout the synthetic process, from the free peptides to the cross-linkers to the scaffolds. It is clear that the proline oligomers are more susceptible to oxidative cleavage rather than their flanking PEG chains. This was supported by GPC measurements that suggested that the PEG-P_n-PEG cross-linkers retained intact PEG structure under MCO conditions (Figure 2). The harsh MCO conditions were chosen because in the presence of copper ions, H_2O_2 can be decomposed into highly reactive hydroxyl radicals.[39]

While the MCO system has been widely employed to mimic oxidative stress in vitro, evidence for its physiological relevance in vivo remain controversial in spite of the availability of plausible mechanisms.[39−41] This is partly because significantly greater concentrations of free metals and H_2O_2 are used in the in vitro model than what is typically found in vivo. Alternatively, the contributions of peroxynitrite ($ONOO^-$) to oxidative stress in vivo are known to be more significant, because of their high reactivity and capability of diffusing across lipid bilayers.[41] Therefore, upon formation of the cross-linked scaffolds, oxidative environments were established via a SIN-1 treatment, since SIN-1 slowly decomposes under aqueous conditions to form O_2^- and $NO^\bullet$ ions, which can very rapidly combine to form $ONOO^-$. This treatment regime produces a more physiologically relevant model of the oxidative stress environment versus the MCO system used in preceding studies. Under these conditions, the presence of proline oligomers within the scaffolds promoted the ROS-responsiveness of the model scaffolds.

Because the scaffolds contained approximately 18% PEG-P_n-PEG by weight, oxidized scaffolds were expected to retain up to ∼82% of their mass (the backbone polymer component) following oxidative treatment. While control PEG-dihydrazide cross-linked scaffolds retained more than 82% of their mass during the study period, the peptide-containing scaffolds retained ∼70%. These findings suggest that oxidative degradation is not limited to the cross-linker components of the scaffolds. Although we selected a 4%PEG-86%PCL-10% cPCL-based polymer to avert this possibility, the PCL/cPCL components are polyesters and therefore, can undergo both hydrolytic and oxidative degradation. These conclusions are consistent with the findings of other groups.[24]

The scaffolds were next incubated with untreated or activated murine macrophages in order to establish the ability of these scaffolds to respond to oxidative stimuli presented in a more physiologically relevant model. SEM and μCT imaging were used to observe changes in the pore architecture of the scaffolds after the 9 d incubation period, and confirmed that PEG-P_7-PEG cross-linked scaffolds, only when incubated with activated macrophages, experienced structural changes and an increase in the occurrence of micropores. Therefore, within this in vitro model of inflammation-related oxidative stress, the activated macrophages degraded the proline oligomer-containing scaffolds more effectively than they did the control scaffolds that were cross-linked with PEG-dihydrazide. This is likely due to increased H_2O_2 production by activated macrophages relative to untreated macrophages. Because of the relatively short study period, complete degradation and disintegration of the scaffolds was not observed.

This is, to our knowledge, the first demonstration of an ROS-mediated, degradable polymeric scaffold, which paves the way for applications in tissue engineering and controlled release where chronic oxidative stress is expected due to disease progression or as a response to implanted materials. The results presented in this study also have widespread implications, because polymeric scaffolds containing peptide-based elements, such as protease-degradable peptide sequences and cell binding motifs, are very widely used.[42−44] In particular, protease-treated hydrogels containing degradable peptide sequences have been shown to degrade significantly over the course of a few days. Because oxidative degradation of peptide-containing scaffolds occurs over longer time frames, this phenomenon is unlikely to significantly affect their proteolytic degradation in vivo. However, our findings suggest that, in applications where an implanted, peptide-containing biomaterial is required to remain viable for months, local ROS production may influence the function and stability of the implant.

In conclusion, we have synthesized polymeric biomaterial scaffolds chemically cross-linked with proline oligomers, which are degradable via local ROS production. These scaffolds may be potentially loaded with drugs and other species for the site-specific therapy of conditions where ROS levels are elevated due to pathogenesis, such as in implant rejection and atherosclerotic plaques. Due to the weeks-to-months time scale required to completely degrade these materials, the use of these materials to treat such conditions, will reduce the necessity for multiple injections or implantation procedures to address the condition.

AUTHOR INFORMATION

Corresponding Author

*Phone: 615-322-6986. Fax: 615-343-7919. E-mail: hak-joon.sung@vanderbilt.edu.

■ ACKNOWLEDGMENTS

We acknowledge the aid of Jason Tucker-Schwartz and Prof. Melissa Skala (both from the Vanderbilt University, Dept. of Biomedical Engineering) for extensive technical help, discussions, and troubleshooting for 3D imaging of the scaffolds in this study. We acknowledge financial support from multiple grants from the National Science Foundation (NSF CAREER CBET 1056046, NSF DMR 1006558), National Institutes of Health (NIH HL091465), and a Vanderbilt University Internal Discovery Grant (4-48-999-9132). R.L.K. acknowledges support through a fellowship through the Vanderbilt University Undergraduate Summer Research Program (VUSRP). SEM was conducted via the core facilities of the Vanderbilt Institute of Nanoscale Sciences and Engineering (VINSE) using facilities renovated under NSF ARI-R2 DMR-0963361.

■ REFERENCES

(1) Halliwell, B.; Clement, M. V.; Long, L. H. *FEBS Lett.* **2000**, *486*, 10−3.
(2) Galis, Z. S.; Sukhova, G. K.; Lark, M. W.; Libby, P. *J. Clin. Invest.* **1994**, *94*, 2493−503.
(3) Scherer, R. L.; McIntyre, J. O.; Matrisian, L. M. *Cancer Metastasis Rev.* **2008**, *27*, 679−90.
(4) Cammas, S.; Suzuki, K.; Sone, C.; Sakurai, Y.; Kataoka, K.; Okano, T. *J. Controlled Release* **1997**, *48*, 157−164.
(5) Gupta, P.; Vermani, K.; Garg, S. *Drug Discovery Today* **2002**, *7*, 569−579.
(6) Fattori, R.; Piva, T. *Lancet* **2003**, *361*, 247−9.
(7) Schmedlen, R. H.; Elbjeirami, W. M.; Gobin, A. S.; West, J. L. *Clin. Plast. Surg.* **2003**, *30*, 507−17.
(8) Tanaka, T.; Decuzzi, P.; Cristofanilli, M.; Sakamoto, J. H.; Tasciotti, E.; Robertson, F. M.; Ferrari, M. *Biomed. Microdevices* **2009**, *11*, 49−63.
(9) Zhang, J. L.; Srivastava, R. S.; Misra, R. D. K. *Langmuir* **2007**, *23*, 6342−6351.
(10) Azuma, H.; Tilney, N. L. *Curr. Opin. Immunol.* **1994**, *6*, 770−776.
(11) Moilanen, E.; Moilanen, T.; Knowles, R.; Charles, I.; Kadoya, Y.; al-Saffar, N.; Revell, P. A.; Moncada, S. *Am. J. Pathol.* **1997**, *150*, 881−7.
(12) Massia, S. P.; Holecko, M. M.; Ehteshami, G. R. *J. Biomed. Mater. Res., Part A* **2004**, *68A*, 177−186.
(13) Napoli, A.; Valentini, M.; Tirelli, N.; Muller, M.; Hubbell, J. A. *Nat. Mater.* **2004**, *3*, 183−9.
(14) Reddy, S. T.; Rehor, A.; Schmoekel, H. G.; Hubbell, J. A.; Swartz, M. A. *J. Controlled Release* **2006**, *112*, 26−34.
(15) Reddy, S. T.; van der Vlies, A. J.; Simeoni, E.; Angeli, V.; Randolph, G. J.; O'Neil, C. P.; Lee, L. K.; Swartz, M. A.; Hubbell, J. A. *Nat. Biotechnol.* **2007**, *25*, 1159−64.
(16) Thomas, S. N.; van der Vlies, A. J.; O'Neil, C. P.; Reddy, S. T.; Yu, S. S.; Giorgio, T. D.; Swartz, M. A.; Hubbell, J. A. *Biomaterials* **2011**, *32*, 2194−203.
(17) Berlett, B. S.; Stadtman, E. R. *J. Biol. Chem.* **1997**, *272*, 20313−6.
(18) Stadtman, E. R.; Berlett, B. S. *Chem. Res. Toxicol.* **1997**, *10*, 485−94.
(19) Amici, A.; Levine, R. L.; Tsai, L.; Stadtman, E. R. *J. Biol. Chem.* **1989**, *264*, 3341−6.
(20) Stadtman, E. R.; Levine, R. L. *Amino Acids* **2003**, *25*, 207−218.
(21) Sung, H. J.; Luk, A.; Murthy, N. S.; Liu, E.; Jois, M.; Joy, A.; Bushman, J.; Moghe, P. V.; Kohn, J. *Soft Matter* **2010**, *6*, 5196−5205.
(22) Sung, H. J.; Su, J.; Berglund, J. D.; Russ, B. V.; Meredith, J. C.; Galis, Z. S. *Biomaterials* **2005**, *26*, 4557−67.
(23) Crowder, S. W.; Gupta, M. K.; Hofmeister, L. H.; Zachman, A. L.; Sung, H.-J. *Acta Biomater.* **2011**, in press.
(24) Ali, S. A. M.; Doherty, P. J.; Williams, D. F. *J. Appl. Polym. Sci.* **1994**, *51*, 1389−1398.
(25) Hermanson, G. T. *Bioconjugate Techniques*, 2nd ed.; Academic Press: San Diego, 2008; p 1323.
(26) Everhart, M. B.; Han, W.; Sherrill, T. P.; Arutiunov, M.; Polosukhin, V. V.; Burke, J. R.; Sadikot, R. T.; Christman, J. W.; Yull, F. E.; Blackwell, T. S. *J. Immunol.* **2006**, *176*, 4995−5005.
(27) Hildebrand, T.; Ruegsegger, P. *J. Microsc. (Oxford, U.K.)* **1997**, *185*, 67−75.
(28) Ruegsegger, P.; Hildebrand, T.; Laib, A.; Muller, R.; Dequeker, J. *J. Bone Miner. Res.* **1999**, *14*, 1167−1174.
(29) Gimenez, S.; Ponsart, S.; Coudane, J.; Vert, M. *J. Bioact. Compat. Polym.* **2001**, *16*, 32−46.
(30) An, S. G.; Cho, C. G. *Macromol. Rapid Commun.* **2004**, *25*, 618−622.
(31) Sung, H. J.; Sakala Labazzo, K. M.; Bolikal, D.; Weiner, M. J.; Zimnisky, R.; Kohn, J. *Eur. Cells Mater.* **2008**, *15*, 77−87.
(32) Hogg, N.; Darley-Usmar, V. M.; Wilson, M. T.; Moncada, S. *Biochem. J.* **1992**, *281*, 419−424.
(33) Sica, A.; Schioppa, T.; Mantovani, A.; Allavena, P. *Eur. J. Cancer (Oxford, U.K.)* **2006**, *42*, 717−727.
(34) Schuessler, H.; Schilling, K. *Int. J. Radiat. Biol.* **1984**, *45*, 267−281.
(35) Mahmoud, E. A.; Sankaranarayanan, J.; Morachis, J. M.; Kim, G.; Almutairi, A. *Bioconjugate Chem.* **2011**, *22*, 1416−21.
(36) Kolb, H. C.; Sharpless, K. B. *Drug Discovery Today* **2003**, *8*, 1128−1137.
(37) Tu, B. P.; Ho-Schleyer, S. C.; Travers, K. J.; Weissman, J. S. *Science* **2000**, *290*, 1571−1574.
(38) Shu, X. Z.; Liu, Y.; Luo, Y.; Roberts, M. C.; Prestwich, G. D. *Biomacromolecules* **2002**, *3*, 1304−1311.
(39) McCall, M. R.; Frei, B. Mechanisms of LDL Oxidation. In *Oxidative Stress and Vascular Disease*, 1st ed.; Keaney, J. F., Jr., Ed.; Kluwer Academic Publishers: Norwell, MA, 2000; pp 75−98.
(40) Stadtman, E. R. *Free Radical Biol. Med.* **1990**, *9*, 315−325.
(41) Murphy, M. P.; Packer, M. A.; Scarlett, J. L.; Martin, S. W. *Gen. Pharmacol.: Vasc. Syst.* **1998**, *31*, 179−186.
(42) West, J. L.; Hubbell, J. A. *Macromolecules* **1998**, *32*, 241−244.
(43) DeLong, S. A.; Gobin, A. S.; West, J. L. *J. Controlled Release* **2005**, *109*, 139−48.
(44) Miller, J. S.; Shen, C. J.; Legant, W. R.; Baranski, J. D.; Blakely, B. L.; Chen, C. S. *Biomaterials* **2010**, *31*, 3736−43.